PHYSICAL REVIEW E VOLUME 53, NUMBER 2 FEBRUARY 1996

Electrodeposition: The role of concentration in the phase diagram and the Hecker transition

O. Zik and E. Moses
Department of Complex Systems, The Weizmann Institute of Science, Rehovot 76100, Israel

(Received 18 January 1995; revised manuscript received 3 November 1995)

We report an experimental study of the morphological phases of zinc electrodeposits. The microscopic morphology is based on two alternative growth mechanisms: tip splitting or dendritic, and is decoupled from the macroscopic structure. The latter is characterized by the density of branches and stability of the front. The key role in the microscopic selection is played by the initial concentration of zinc. The importance of ion availability is manifested again in the Hecker transition, where the departure from dense branching morphology coincides with the exhaustion of zinc from the original solution.

PACS number(s): 68.70.+w, 47.20.Hw, 05.70.Fh, 81.10.Dn

Nonequilibrium growth phenomena arise in numerous systems. Familiar examples are solidification, viscous fingering, bacterial growth, and electrochemical deposition [1]. These systems exhibit a large variety of patterns, referred to as morphological phases. The selection of a distinct morphology, e.g., dendritic, dense branching (DBM), or diffusion limited aggregation (DLA) [2] is still the focus of many studies. Quasi-two-dimensional electrodeposition is especially interesting in this context. This system exhibits a wide variety of morphologies and is relatively easy to control. These properties motivated a number of works, aimed to classify the different morphologies as a function of the physical parameters. In 1986 Grier *et al.* [3] and Sawada, Dougherty, and Gollub [4] independently studied the morphological phase diagram of zinc sulfate in a circular geometry, using the electrolyte concentration and applied potential as control parameters. Despite the similarity between the two experiments, the resulting diagrams are qualitatively different. Later attempts along this line, using copper electrodes and a parallel geometry, produced more dissimilar results [5]. The discrepancy might be due to the influence of surface active impurities, as suggested by Brady and Ball [6], or the presence of free protons [7] and dissolved oxygen, as suggested by others [8,9]. The particular geometry (rectangular or circular) and cell dimensions were also found to play a role in the morphology selection [7,9]. Our goal is to clarify this point as well as gain insight into the physics of the morphological phases and the transitions between them. It seems that despite an illusive correspondence between electrodeposition and the DLA model, the more interesting questions refer to the role of convection [10,11] and the influence of impurities on the crystallization.

Essential to our success is the ability to minimize the variations in the driving force during growth. Thus, we use a rectangular geometry and constant current. This configuration, previously used to study other aspects of the system [12,13], allows us to maintain a constant deposition velocity. The two main experimental problems are the sensitivity to chemical conditions and the variation in spatiotemporal behavior within a single experimental run [12]. Our answer is to standardize sample preparation and experimental procedure, and consider only the steady-state morphology in the concentration-current parameter plane.

An interesting phenomenon, unique to electrodeposition, is the Hecker transition. Despite the extensive effort devoted to its study [7,8,14,15], the number of transitions and the origin of each are still a matter of controversy. This effect is generally described as a sudden change in the density of branches and/or other properties of the growing deposit. The location of the transition, be it one half or 90% [14] of the electrode separation, was found to scale with this distance, indicating that the transition is a finite-size effect. Recent experimental and theoretical studies support this conclusion [15]. So far there are five distinct morphological transitions reported in the literature, each appearing at a fixed fraction of the electrode separation. This property is consistent with the explanation given by Fluery, Rosso, and Chazalviel [7] who interpreted the transition as the influence of a migrating cationic front. Our experiments show that the Hecker effect coincides with the exhaustion of the original solution.

The experiment is conducted in a cell consisting of two thick (0.5 cm) glass plates of dimensions 7×5 cm. Sandwiched between them are two thin (typically 0.15 mm), 5-cm-long and 4.5-cm-apart zinc (99.9%) electrodes that act as spacers. The volume bounded by the glass plates and electrodes is filled with aqueous solution of zinc sulfate (BDH, 99.5% $ZnSO_4 \cdot 7H_2O$, in 18.1-MΩ/cm ultrapure water). The solution is stored in sealed containers, to minimize the effect of aging due to dissolved atmospheric gases [12], and is used to rinse the cell before use. The cell is coupled to a thermal bath (Neslab RTE-220) to maintain a constant (23.0 °C) temperature. This reduces the effect of temperature variations, which are expected to play a role where they are least desired, that is, near the interface. There the depletion of ion increases the electrical resistivity and consequently Ohmic heating. The growth is driven by a constant current source (Keithley 222). A typical run is terminated when the voltage between cathode and anode reaches the current source limit (105 V) or when the deposit arrives at the cathode. The Ohmic resistance changes due to two competing effects: depletion of ions and the narrowing of the effective gap between anode and deposit. Several runs that required higher voltages, i.e., at very low concentration or high currents, were performed using the current regulation mode of a dc power supply (Lambda LPD 425, allowing up to 500 V dc).

About 100 experimental runs were performed with fixed current and initial electrolyte concentration, ranging from 0.1 to 30 mA and 0.01*M* to 1*M*, respectively. These values explore most of the available phase space. Its limits are primarily determined by two processes: intervention of hydrogen bubbles, which takes place at high currents and at low concentrations, and the formation of a zinc hydroxide layer [12] followed by the growth of a three-dimensional structureless deposit, which appears at low currents. Within these limits, the deposit can be decomposed into distinct main branches stemming from near the cathode. It is natural to define a "microstructure" relating to the sub-branching structure of the individual main branch (e.g., dendritic) and a "macrostructure" relating to the morphology of the collection of main branches (e.g., sparse or dense branches).

Figure 1 shows the morphological phase diagram within these limits. Not all macroscopic effects were included in the diagram, and we ignore some quantitative features like the thickness and number of branches, which are also influenced by the control parameters. For example, the dendrites tend to be narrower and sharper at high currents (corresponding to the previously reported "stringy" phase [3]) and thicker at high concentrations. Our work focuses rather on the more qualitative properties that reflect the microscopic growth mechanism. The phase diagram thus obtained consists of a number of clear portions, which we classify as follows:

(I) Dendritic [Fig. 2(a)]—appearing at high concentra-

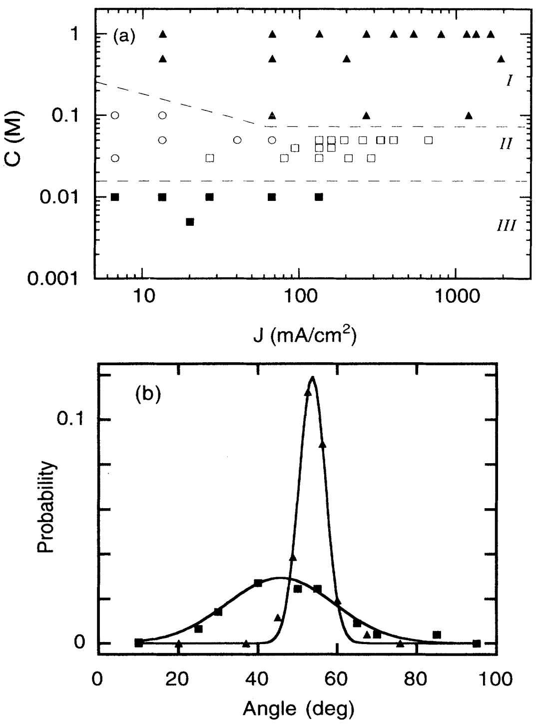

FIG. 1. (a) The current (J) vs. concentration (C) phase diagram. Each point is the result of 2–3 experimental runs. The different morphologies are represented as follows (see text for details): dendritic, full triangles; tip splitting, full squares; mixed, empty circles; DBM, empty squares. These results show that the concentration plays the key role in the microscopic morphology selection. (b) The branching angle probability for the dendritic and tip splitting regimes. The mean and standard deviation are $53.7\pm0.1^\circ$ and $3.4\pm0.1^\circ$, respectively for the dendritic angular probability distribution and $46.0\pm0.9^\circ$ and $14.0\pm0.7^\circ$, respectively for the tip splitting one.

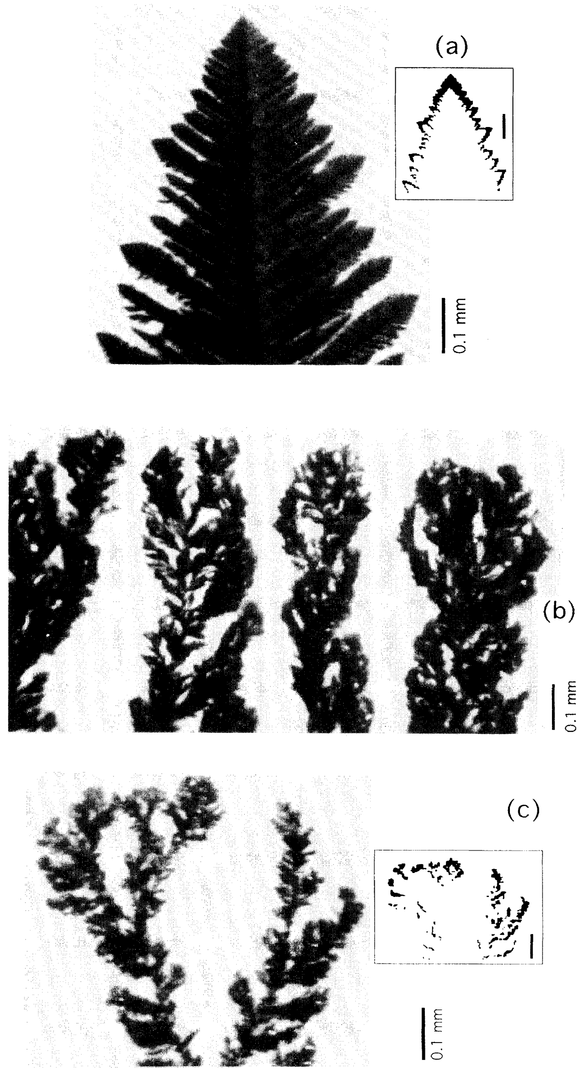

FIG. 2. Typical morphologies of zinc electrodeposits: (a) dendritic ($C=0.1M, J=10$ mA/cm^2), (b) DBM (0.03*M*, 60 mA/cm^2), (c) tip splitting (0.01*M*, 10 mA/cm^2). The reduced pictures in the insets in (a) and (c) are the result of image subtraction, which illustrates the cluster size distribution function. [The time difference is 0.5 s in (a) and 1.5 s in (c).] In the dendritic regime one sees that the growth is more connected.

tions. Microstructure characterized by its backbone, preferentially oriented along the propagation direction. The side branching is equally spaced, narrowly peaked around 53° [see Fig. 1(b)].

(II) Transition regime—appearing at intermediate concentrations. At low currents microstructures coexist in this region—dendrites and tip splitting appear in different parts of the cell. At high currents a dense branching morphology appears [Fig. 2(b)], with either dendritic or tip splitting microstructure.

(III) Tip splitting [Fig. 2(c)]—appearing at low concentrations. Microstructure characterized by no backbone, and widely distributed branching angles [see Fig. 1(b)], apparently similar to the outcome of a DLA process.

This classification represents the experimentally observed decoupling of microscopic (tip splitting or dendritic) and macroscopic morphologies. Regimes (I) and (III) are characterized by different *microstructures* and are selected by the concentration, regardless of the current. In the transition regime (II) the current affects the *macrostructure*. This may consist of densely packed branches, defining a stable (DBM) front, as observed at intermediate concentrations and high currents, or sparse branches and unstable front at lower currents.

A quantitative distinction between the dendritic and tip splitting regimes is given by the probability distribution function of branching angles, shown in Fig. 1(b). Other methods, such as cluster size distribution function [see the insets in Figs. 2(a) and 2(c)] and fractal dimension gave a clear distinction between regimes, but were more sensitive to experimental noise. The angular distribution in the tip splitting regime is about 4 times wider than in the dendritic phase.

Typical branches of the dendritic and tip splitting phases are shown in Figs. 2(a) and 2(c), respectively. The dendritic phase consists of a number of main trunks that retain integrity during growth. The side branching angle is a signature of the crystalline close packing of zinc. In contrast, the tip splitting phase grows by recurrent tip splitting with little correlations between the branching angles. This result can be interpreted as follows: the generic morphology of zinc electrodeposits, which arises from its crystalline anisotropy, is dendritic (see Argoul and Kuhn [12]). This state is altered at low concentrations, where the reduced availability of zinc and the constraint of constant electric current lead to electroconvection. The resulting fluid motion is marked in our experiment by the fluctuating transverse movement of the growing branches. It involves convection rolls near the tips, which yield tip splitting [16,17]. This interpretation is consistent with the theoretical analysis of Bruinsma and Alexander [10], who concluded that small currents are sufficient to generate electroconvection, depending on the material properties.

Two phases are observed in the intermediate concentration regimes (0.025*M* to 0.05*M*). At low currents a mixture of tip splitting and dendritic growth occurs. That is, the deposit in different parts of the cell grow differently within the same run. This may occur simultaneously or with alternating transitions as observed pre-

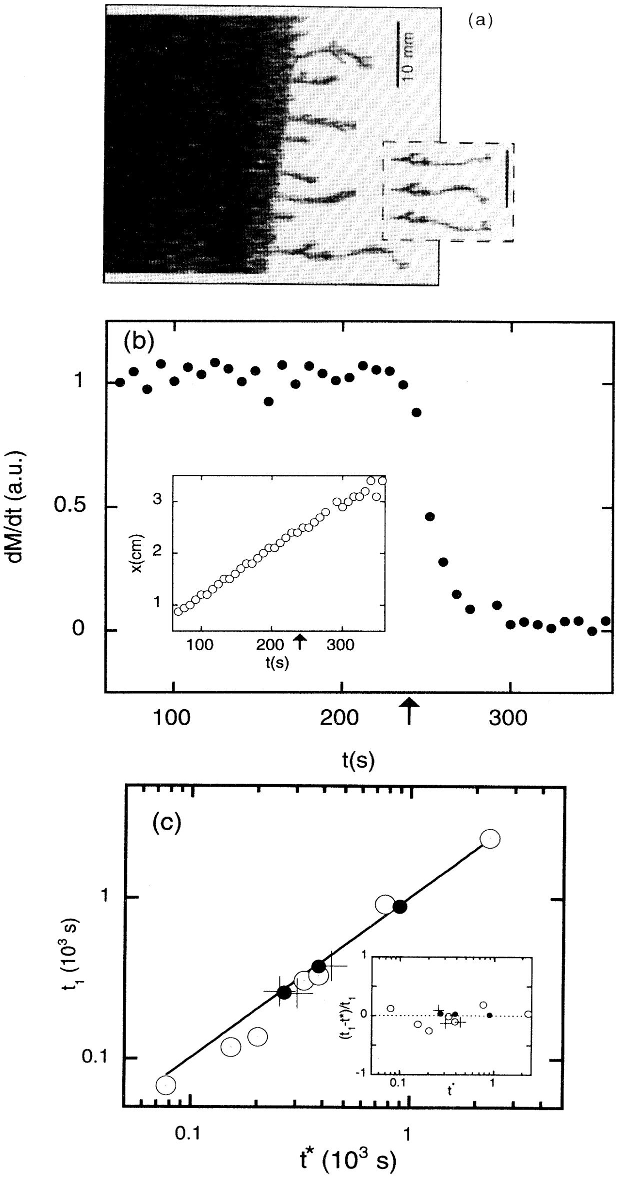

FIG. 3. DBM followed by the Hecker transition (0.03*M*, 100 mA/cm^2). Notice the sharp decrease in the number of branches at the transition. The straight lines in (a) indicate the cell boundaries. The inset contains a collage of three consecutive (1 s) snapshots of the lowest branch. Its motion marks strong convection currents. The corresponding decrease in the cluster (or "mass") deposition rate dM/dt (in pixels) is shown in (b). The units are arbitrary since the thickness of the deposit is not monitored. The first 50 s include a transient during which the front stabilizes from the initial conditions of the specific run, and are omitted for the sake of clarity. The arrows near the abscissa indicate the calculated transition time t^* (cell dimensions: $5\times 4.5\times 0.017$ cm^3). The inset presents the position of the interface as a function of time, showing that the velocity is constant and remains so after the transition. In (c) we show that the two times t^* and t_1 coincide over a range of J and C values: 0.03*M*, open circles; 0.0335*M*, full circles; 0.04*M*, crosses. The straight line is the best linear fit. The inset shows the deviation $(t_1-t^*)/t_1$.

viously [18]. At high currents we observed the dense branching morphology, which appears as macroscopically ordered, equally spaced branches, growing with a front parallel to the anode [3,4,8,19] [Fig. 2(b)]. In the DBM regime we observed that at higher concentrations the individual branch tends to be more "dendritic." This again suggests that the macroscopic and microscopic morphologies are driven by different mechanisms.

The DBM growth leads to the Hecker transition. Its typical manifestation is a sudden decrease in the number of branches (by a factor that ranges between 3 to 7), at about the center of the cell, as shown in Fig. 3(a). Since we apply constant current, the natural assumption is that the growth velocity will consequently increase to maintain the rate of charge transfer. In Fig. 3(b) we show that this is not the case. The sharp decrease of the mass deposition rate, while keeping the charge transfer constant, implies that the origin of the current after the transition is not the electrodeposition of zinc. Once the zinc ions are exhausted, the applied electric field induces other chemical processes, such as reduction of protons and oxygen (see Argoul and Kuhn [12]). Charge transfer is then supplemented by the motion of nonzinc charge carriers such as protons. Beyond the transition we observe strong convection currents, as shown in the inset in Fig. 3(a). These are a manifestation of the electroconvection, which arises when the zinc ions can no longer account for the forced current.

Motivated by the connection between the Hecker effect and the reduced availability of zinc ions, we study the relation between the occurrence of the transition and the exhaustion time of the original solution (without the contribution of the dissolving anode). In Fig. 3(c) we compare the expected exhaustion time t^* with the growth time t_1 (measured from initiation of growth, typically 2–4 s after power on, to the transition). The first is $t^* = Q/I$, where Q is the total charge of free zinc ions in the solution and I the applied current. The second is $t_1 = L/V$, where L is the location of the transition and V the front velocity. This representation enables a compact display of several runs, performed at different concentrations ($0.025M$–$0.04M$) and various current densities. The slope is 1.04 ± 0.13 showing that the two processes coincide.

Another measurement of the same effect is to weigh the amount of deposited zinc up to the transition point. The result of 15 runs (in concentration $0.03M$, current ranging from 5 to 10 mA and cell volume of $5 \times 4.6 \times 0.026$ cm^3) is 1.2 ± 0.1 mg while the weight of the original ions is 1.17 mg. For comparison in the dendritic regime at $0.5M$ and 10 mA the deposit weighs less than 0.1 mg.

A number of results from recent experiments can be tied in to our results. The role of exhaustion of the original ions in solution, and the transition to ions from the dissolving anode has been hinted at previously. Fleury, Rosso, and Chazalviel [7] showed that the anode composition determines the ion content in the deposit after the transition. In the case of a molybdenum anode, which does not dissolve, the deposit just stops once the original ion content is exhausted. In the case of a copper anode, the deposit has a reddish tint after the transition, indicating that copper ions participate in the growth. Furthermore, the exhaustion times t_1 and t^* calculated at their second transition, coincide.

Kuhn and Argoul [8] have shown that the addition of alkali-metal ion impurities promotes the production of the DBM and the subsequent occurrence of the Hecker transition. Minute amounts of impurities are found even in our ultrapure zinc sample (0.001 % by weight each of sodium, potassium, and calcium impurities). The DBM phase is denser than the sparse one by 1–2 orders of magnitude, dense enough to deplete the zinc ions of the original solution.

Finally, the recent work of Huth *et al.* [11], although not directly related to our work, has potential implication on it. Large-scale flow in convective roles on the scale of the cell size was visualized and shown to be dominant in determining the propagation of the various fronts in the cell. Applying this method to the Hecker regime should shed further light on our results.

To summarize, we found that the morphology selection of zinc electrodeposits under constant current is dominated by the initial solution concentration. Ordered structures are obtained at high concentrations, while at low concentrations the growth is characterized by disordered structures that are created by tip splitting. The key role of ion availability is manifested again in the intermediate-concentration–high-current regime where the macroscopic structure exhibits a dense morphology with a stable front. The Hecker transition, which then occurs, coincides with the exhaustion of the original solution.

We would like to thank R. Zeitak and O. Krichevsky for fruitful discussions and V. Steinberg for reading the manuscript. This work was supported by the Gabriel Alhadeff research award, the Minerva Foundation, Munich, and the Minerva Center for Nonlinear Physics.

---

[1] T. Viscek, *Fractal Growth Phenomena* (World Scientific, Singapore, 1992).
[2] T. Witten and L. M. Sander, Phys. Rev. Lett. **47**, 1400 (1981).
[3] D. Grier, E. Ben-Jacob, R. Clarke, and L. M. Sander, Phys. Rev. Lett. **56**, 1264 (1986).
[4] Y. Sawada, A. Dougherty, and J. P. Gollub, Phys. Rev. Lett. **56**, 1260 (1986).
[5] P. P. Trigueros, J. Claret, F. Mas, and F. Sagues, J. Electroanal. Chem. **312**, 219 (1991).

[6] R. M. Brady and R. C. Ball, Nature **309**, 225 (1984).

[7] V. Fleury, M. Rosso, and J. N. Chazalviel, Phys. Rev. A **43**, 6908 (1991).

[8] A. Kuhn and F. Argoul, Phys. Rev. E **49**, 4298 (1994).

[9] M. A. Guzman, R. D. Feimuth, P. U. Pendse, M. C. Veindt, and L. Lam, in *Nonlinear Structures in Physical Systems,* edited by L. Lam and H. C. Moris (Springer, New York, 1990).

[10] R. Bruinsma and S. Alexander, J. Chem. Phys. **92**, 3074 (1990).

[11] J. M. Huth, H. L. Swinney, W. D. McCormick, A. Kuhn, and F. Argoul, Phys. Rev. E **51**, 3444 (1995).

[12] F. Argoul and A. Kuhn, J. Electroanal. Chem. **359**, 81 (1993).

[13] V. Fleury, M. Rosso, J. Chazalviel, and B. Sapoval, Phys. Rev. A **44**, 6993 (1991).

[14] J. R. Melrose, D. B. Hilbert, and R. C. Ball, Phys. Rev. Lett. **65**, 3009 (1990).

[15] V. Fleury, J. H. Kaufman, and D. B. Hilbert, Nature **367**, 435 (1994).

[16] D. Barkey, D. Watt, Z. Liu, and S. Raber, J. Electrochem. Soc. **139**, 1044 (1994).

[17] V. Fleury, J. Chazalviel, and M. Rosso, Phys. Rev. Lett. **68**, 2492 (1992).

[18] M. Wang and N.-b. Ming, Phys. Rev. Lett. **71**, 113 (1993).

[19] P. P. Trigueros, J. Claret, F. Mas, and F. Sagues, J. Electroanal. Chem. **328**, 165 (1992).

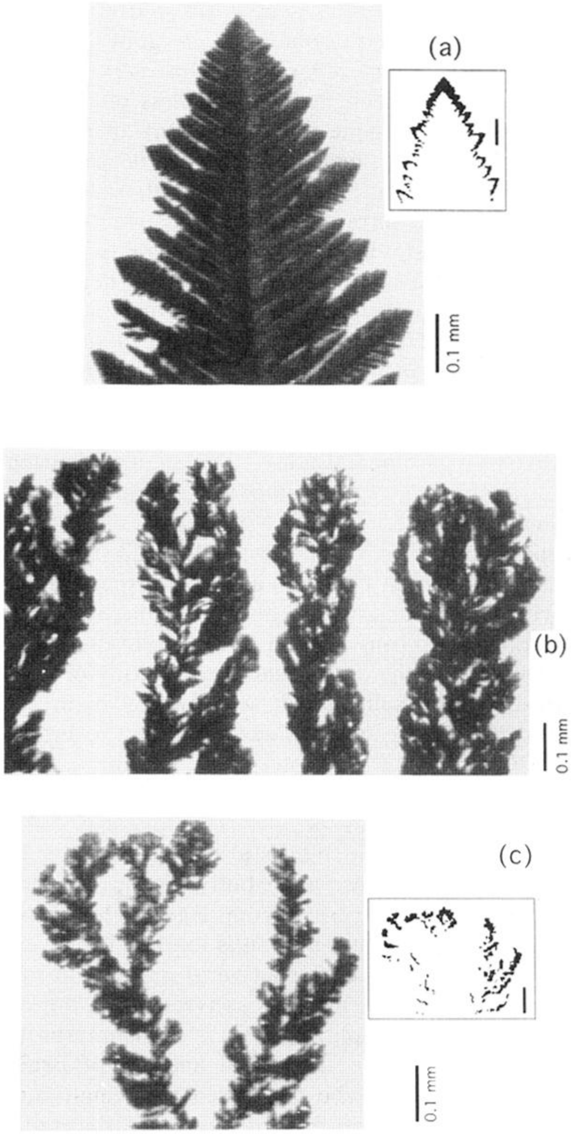

FIG. 2. Typical morphologies of zinc electrodeposits: (a) dendritic ($C = 0.1M, J = 10$ mA/cm^2), (b) DBM (0.03M, 60 mA/cm^2), (c) tip splitting (0.01M, 10 mA/cm^2). The reduced pictures in the insets in (a) and (c) are the result of image subtraction, which illustrates the cluster size distribution function. [The time difference is 0.5 s in (a) and 1.5 s in (c).] In the dendritic regime one sees that the growth is more connected.

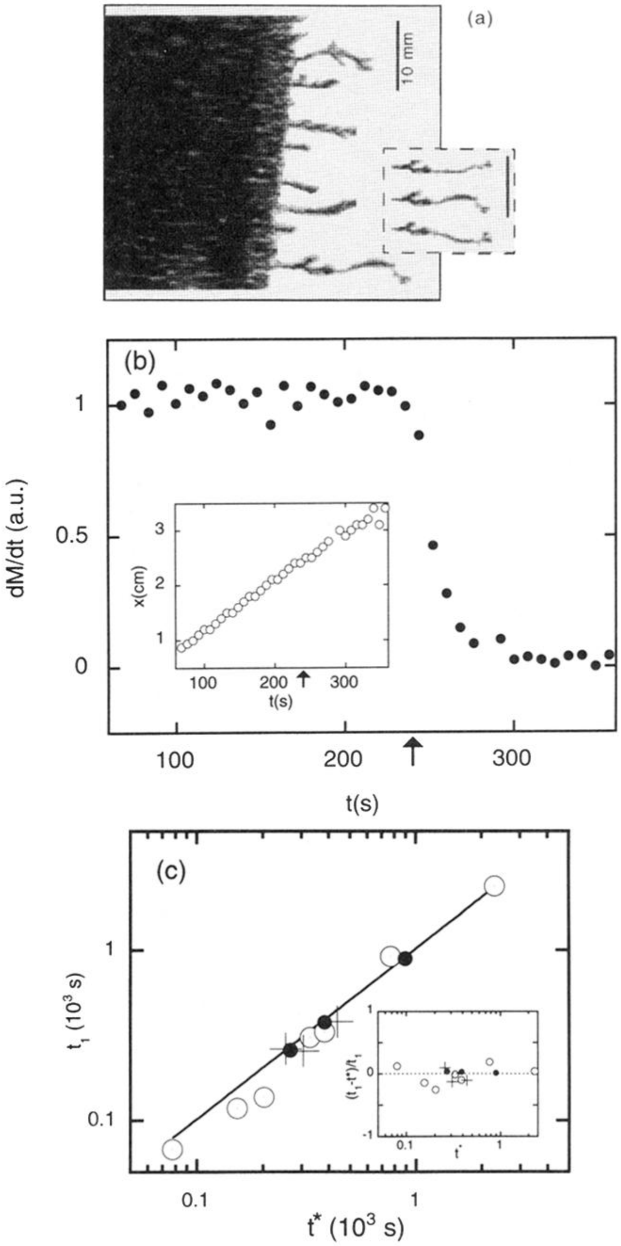

FIG. 3. DBM followed by the Hecker transition (0.03M, 100 mA/cm^2). Notice the sharp decrease in the number of branches at the transition. The straight lines in (a) indicate the cell boundaries. The inset contains a collage of three consecutive (1 s) snapshots of the lowest branch. Its motion marks strong convection currents. The corresponding decrease in the cluster (or "mass") deposition rate dM/dt (in pixels) is shown in (b). The units are arbitrary since the thickness of the deposit is not monitored. The first 50 s include a transient during which the front stabilizes from the initial conditions of the specific run, and are omitted for the sake of clarity. The arrows near the abscissa indicate the calculated transition time t^* (cell dimensions: $5\times4.5\times0.017$ cm^3). The inset presents the position of the interface as a function of time, showing that the velocity is constant and remains so after the transition. In (c) we show that the two times t^* and t_1 coincide over a range of J and C values: 0.03M, open circles; 0.0335M, full circles; 0.04M, crosses. The straight line is the best linear fit. The inset shows the deviation $(t_1-t^*)/t_1$.